JOURNAL OF THERMOPHYSICS AND HEAT TRANSFER
Vol. 6, No. 4, Oct.–Dec. 1992

Prediction of Radiative Transfer in Cylindrical Enclosures with the Finite Volume Method

E. H. Chui* and G. D. Raithby†
University of Waterloo, Waterloo, Ontario N2L 5J8, Canada
and
P. M. J. Hughes‡
Energy Research Laboratories, CANMET, Ottawa, Ontario K1A 0G1, Canada

This article shows how the finite volume method can be implemented to solve three-dimensional radiation problems in cylindrical enclosures. The medium is considered to be gray, and absorption, emission, and either isotropic or nonisotropic scattering are included. For the special case of axisymmetric radiation, a mapping is described that yields a complete solution by solving the intensity in a single azimuthal direction. The method is shown to rapidly converge to the solution of the radiation transfer equation as the spatial and directional grid is refined. Results from the solution of axisymmetric bench mark problems show that the method is stable, accurate, and computationally efficient.

Nomenclature

A = area, m^2
D_f^l = direction cosine to surface normal integrated over ω^l [Eq. (3)]
$I(\boldsymbol{R}, s)$ = radiant intensity, W/(m^2 sr)
$\bar{I}(\boldsymbol{R}, s)$ = inscattering term at $\boldsymbol{R}$ in direction s [Eqs. (2) and (8b)]
$\bar{I}^l$ = inscattering term for solid angle ω^l [Eq. (8a)]
I_b = blackbody intensity, W/(m^2 sr)
I_f^l = intensity at integration point f within ω^l, W/(m^2 sr)
I_P^l = intensity at node P within ω^l, W/(m^2 sr)
I_{uf}^l = upstream intensity for integration point f within ω^l, W/(m^2 sr)
K_a = absorption coefficient, m^{-1}
N_r, N_z = number of control volumes in the r and z directions, respectively
N_θ, N_ϕ = number of discrete angles in polar θ, and azimuthal ϕ directions
$\boldsymbol{n}$ = outward unit normal to a surface
q = radiant heat flux, W/m^2
$\boldsymbol{q}$ = radiant heat flux vector, W/m^2
R = the intensity source function [Eq. (6)]
$\boldsymbol{R}$ = position vector
r = radius in the (x, y) plane, m
S = path length, m
s = unit vector in direction of intensity
T = temperature, K
V = volume, m^3
x', y', z' = directions parallel to the x, y, and z axes (Fig. 1)
ε = surface emissivity
θ = polar angle measured from the z direction
κ = extinction coefficient [Eq. (6)]
σ = Stefan-Boltzmann const
σ_s = scattering coefficient, m^{-1}
Φ = scattering phase function, Eq. (2)
$\bar{\Phi}$ = new variable for phase function, Eq. (8b)
ϕ = azimuthal angle measured from the radial direction (Fig. 1)
φ = azimuthal angle measured from the x' axis (Fig. 1)
ψ = scattering angle between incident and scattered directions
ω = solid angle, sr
ω_s = scattering albedo

Subscripts
B = boundary
b = blackbody
f = integration point f on the surface of a control volume
g = association with medium
P = nodal point P
r = radial direction
u = upstream position
w = boundary

Superscripts
$*$ = dummy variable or a nondimensional quantity
l = association with solid angle ω^l
l^-, l^+ = boundaries of solid angle ω^l

Received July 2, 1991; revision received Dec. 13, 1991; accepted for publication Dec. 13, 1991.

*Ph.D. (1990), Department of Mechanical Engineering.
†Professor, Department of Mechanical Engineering.
‡Research Scientist.

Introduction

AXISYMMETRIC radiative transfer in cylindrical enclosures has been studied by a substantial number of researchers, and almost every radiation model has been applied to this type of problem [e.g., Monte Carlo method (Perlmutter and Howell[1]), flux method (Lowes et al.[2]), zone method (Steward and Tennankora[3]), discrete ordinates method (Fiveland[4]), Galerkin finite element method (Fernandes and Francis[5]), and spherical harmonic method (Mengüç and Viskanta[6])]. As an additional small sample of the extensive recent literature on this problem, the reader may consult Jamaluddin and Smith,[7] Yucel and Williams,[8] and Carvalho et al.[9] There is such widespread interest in axisymmetric radiation because it allows the performance of radiation models to be assessed on simple problems, and because radiation in boilers, furnaces, and combustors can sometimes be modeled as axisymmetric.

From recent reviews by Howell[10] and Viskanta and Mengüç,[11] it is evident that no single radiation model can be re-

garded as the best for all problems. In the context of modeling reacting flows, the flux methods are often adopted because of their compatibility with the numerical algorithms used for solving the fluid dynamics equations. The spherical harmonics (P_3) method and the discrete ordinates (S_N) method are generally more accurate than the simple four or six flux models, but they too have shortcomings.[6,12] The need for better models still exists.

Raithby and Chui[13] recently proposed a finite volume method (FVM) that shares the same philosophy and grid as the finite volume techniques currently used in predicting fluid flow and convective heat transfer. In this method the computational domain is subdivided into discrete (finite) volumes, and direction is subdivided into discrete solid angles. The radiation transfer equation (RTE) integrated over both a discrete volume and solid angle serves as the starting point.

Although this method has many similarities to the discrete ordinates method, it does not use the quadrature that gives rise to the discrete ordinates. The discrete ordinates method is also usually applied by approximating derivatives in the RTE by finite differences, although Fiveland[14] recently started from volume-integrated equation. By starting with the integral of the RTE over both discrete angles and volumes, the FVM avoids "ray effects"[15] by guaranteeing exact global conservation of radiant energy. Total inscattering is also exactly balanced by total outscattering for each finite volume for any phase function. Whereas the discrete ordinates method has, to the authors' knowledge, only been applied on Cartesian and circular-cylinder computational grids, the FVM was designed for use on virtually any of the grid types that are currently used to compute fluid flow.

There are, of course, many ways to implement a FVM. The particular implementation of the FVM used by Raithby and Chui[13] exactly captured the diffusion limit for strongly participating media, and reduced nonphysical "wiggles" in the solution, by use of a special discretization approximation. Although somewhat algebraically complex, this variant was shown to be stable, accurate, and computationally efficient for rectangular enclosures.

In this article a particular implementation of the general FVM is described that applies to spatially three-dimensional radiation problems on a circular-cylinder mesh. The medium may be absorbing, emitting, and isotropically or anisotropically scattering. This method is applied to axisymmetric problems involving cylindrical enclosures of finite length. The contributions of this article include 1) a new discretization scheme for three-dimensional problems; 2) a less restrictive treatment of scattering than previous methods; 3) a mapping that simplifies the solution of axisymmetric problems; and 4) a demonstration of performance of the method for axisymmetric problems. The gray gas approximation is implicitly used throughout the present article.

It may be helpful to explain why a general three-dimensional model is described in a paper where the focus is on axisymmetric problems. The main reason is that it is simpler to draw the diagrams and explain the method for the general three-dimensional case, and all the material presented is needed for the axisymmetric problem. The second reason is that the three-dimensional model applies to any problem for which the mesh is orthogonal, so may be itself of interest. Results for the general three-dimensional model have not been provided to avoid diffusing the focus of this article.

Governing Equation

The basis for quantitative studies of radiative heat transfer is the RTE. For a gray medium, the RTE has the form (see Siegel and Howell[16])

$$\frac{dI(\boldsymbol{R}, \boldsymbol{s})}{ds} = -(K_a + \sigma_s)I(\boldsymbol{R}, \boldsymbol{s}) + K_a I_b(\boldsymbol{R}) + \sigma_s \bar{I}(\boldsymbol{R}, \boldsymbol{s}) \tag{1}$$

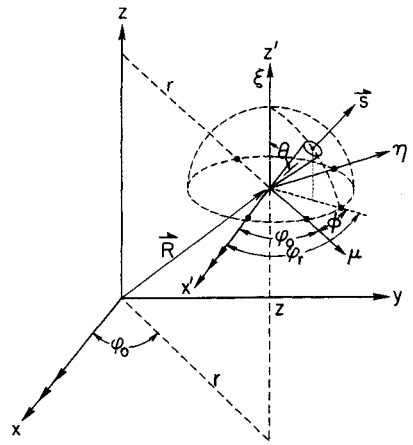

Fig. 1 Cylindrical coordinates for the equation of radiative transfer.

This equation describes the increase in radiant intensity $I(\boldsymbol{R}, \boldsymbol{s})$ at spatial location $\boldsymbol{R}$ over the path length ds in the direction of unit vector $\boldsymbol{s}$, as shown in Fig. 1. The first and third terms on the right side of Eq. (1) represent the effects of absorption and emission, respectively. "Outscattering," term two, reduces the intensity in the $\boldsymbol{s}$ direction, while "inscattering," term four, redirects energy from other directions into the $\boldsymbol{s}$ direction. The inscattering term is defined by

$$\sigma_s \bar{I}(\boldsymbol{R}, \boldsymbol{s}) = \frac{\sigma_s}{4\pi} \int_{4\pi} I(\boldsymbol{R}, \boldsymbol{s}')\Phi(\boldsymbol{s}, \boldsymbol{s}')\, d\omega' \tag{2}$$

where the fraction of the intensity $I(\boldsymbol{R}, \boldsymbol{s}')$ in direction $\boldsymbol{s}'$ that is scattered into direction $\boldsymbol{s}'$ is defined by the phase function $\Phi(\boldsymbol{s}, \boldsymbol{s}')$.

Finite Volume Solution of the RTE

Discrete Energy Balance

Equation (1) expresses the conservation of radiant energy in direction $\boldsymbol{s}$ over an infinitesimal control volume and within an infinitesimal solid angle. The FVM yields an approximate (discrete) solution to this equation which converges to the solution of Eq. (1) as the computational grid is refined.

To implement the method, the computational domain is divided into volumes by a computational mesh. Figures 2a and 2b show a typical subdivision for a cylindrical enclosure. Furthermore, direction is subdivided into discrete solid angles ω^l with each one defined by a particular range of angles θ and ϕ in Fig. 1. The intensity within the volume centered at P and within ω^l is represented by a single value I_P^l. The equation for I_P^l is the RTE integrated over the volume V_P and over ω^l.

The control volume centered at P in Fig. 2 is redrawn in Fig. 3a. The "integration points" $f = 1, 2, \ldots, 6$ lie on the volume faces, at the intersection of the coordinate surfaces that pass through the nodes. The radiant energy Q_f^l, which lies within ω^l and that crosses face f of area A_f, is approximated by

$$Q_f^l = I_f^l A_f \int_{\omega^l} \boldsymbol{s}\cdot\boldsymbol{n}_f\, d\omega = I_f^l A_f D_f^l \tag{3}$$

where I_f^l and $\boldsymbol{n}_f$ (the unit surface normal) at point f are used to approximate their values across the control volume surface A_f. D_f^l is evaluated analytically.

Integration of the RTE over V_P and ω^l (see Raithby and Chui[13]) results in the conservation constraint so that the net radiant flux leaving through the surfaces of V_P within ω^l equals the net "generation" of radiant energy within V_P and ω^l by emission, absorption, inscattering, and outscattering. Ap-

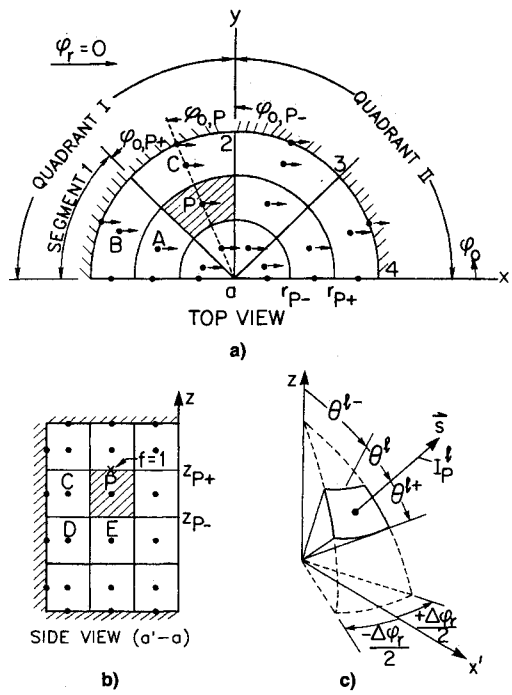

Fig. 2 Schematic of a cylindrical enclosure with a three-dimensional computational grid: a) top view; b) side view; c) typical discrete solid angle.

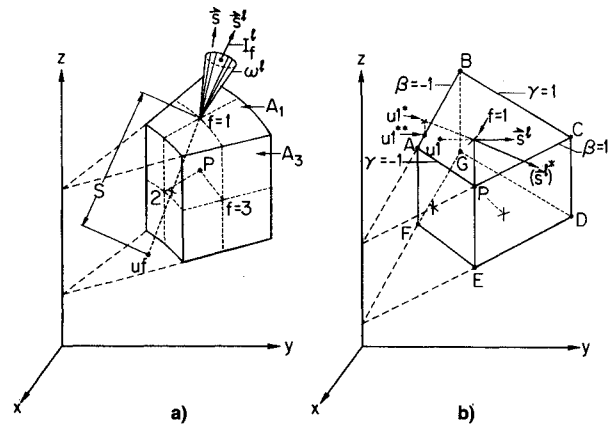

Fig. 3 Typical control volume in a cylindrical enclosure with P located at the center: a) area A_f and intensity I_f^l on one discrete surface panel and integration points f = 1, 2, 3, and b) molecule of nodal points adjacent to node P.

proximating the generation term using nodal-point values of intensity, this conservation balance becomes

$$\sum_{f=1}^{6} Q_f^l = \sum_{f=1}^{6} I_f^l A_f D_f^l$$

$$= [K_{a,P} I_{b,P} - (K_{a,P} + \sigma_{s,P}) I_P^l + \sigma_{s,P} \bar{I}_P^l] V_P \omega^l \qquad (4)$$

For this to be a useful equation for I_P^l, the integration point values I_f^l must be related to nodal point values of I^l. This is discussed in the next section.

Evaluation of I_f^l

If the intensity I_{uf} at some point uf that lies distance S "upstream" of f along the direction s^l (see Fig. 3a) were known, the RTE could be integrated to relate I_f^l to I_{uf}^l. The actual value of I_f^l would depend on the processes affecting the radiation as it passes from uf to f. Representing these processes by a two-term Taylor series expansion about point f, Raithby and Chui[13] showed that

$$I_f^l = I_{uf}^l e^{-\kappa_f S} + R_f^l (1 - e^{-\kappa_f S})$$

$$- \frac{1}{\kappa_f} \left(\frac{\partial R^l}{\partial s^l} \right)_f [1 - e^{-\kappa_f S}(1 + \kappa_f S)] \qquad (5)$$

where the extinction coefficient κ and variable R^l are defined as

$$\kappa = K_a + \sigma_s \qquad R^l = \frac{K_a I_b + \sigma_s \bar{I}^l}{\kappa} \qquad (6)$$

Retention of the last term in Eq. (5) is crucial if the FVM is to reduce exactly to the diffusion model of radiation for large κ.

In providing an equation for I_f^l, Eq. (5) introduces the new unknowns I_{uf}^l, R_f^l and the directional derivative $(\partial R^l/\partial s^l)_f$. A method of evaluating I_{uf}^l is now introduced.

The control volume in Fig. 3a is a perspective view of the control volume centred at P in Fig. 2, for which five of the 27 neighbor nodes are A, B, C, D, and E. The location of the integration point f = 1 in Figs. 2b and 3a, as well as several nodes, are shown in Fig. 3b. It is important to note that the surface A-B-C-P in Fig. 3b is not a control-volume surface, but is rather a surface of constant z that passes through the nodes. The point f = 1 lies on the control volume surface. The dashed line that passes through the point f = 1 in Fig. 3b lies in the direction of s^l, and intersects the surface A-B-C-P at point $u1$. The value of I_{u1}^l is approximated from the surrounding nodal point values of I^l (i.e., I_P^l, I_A^l, I_B^l, I_C^l) using bilinear interpolation,[17] which requires use of a local β, γ coordinate system where $\gamma = \pm 1$ and $\beta = \pm 1$ on the boundaries shown in Fig. 3b.

For some directions, for example $(s^l)^*$ in Fig. 3b, the upstream intersection $u1^*$ falls on the extension of the plane A-B-G-F, so the above prescription must be modified if the computational molecule is to be kept simple. For this case, $I_{u1^*}^l$ is replaced by $I_{u1^{**}}^l$, where $u1^{**}$ is the projection along the z axis, onto the A-B-C-P plane, and where its value is found by linear interpolation.

A similar strategy is followed for other solid angles ω^l and for other integration points (f = 2, 3, . . . , 6). The general rule for locating I_{uf}^l for any control volume P is that no interpolation should be done using nodes that lie "downstream" of P. This practice yields an algebraic equation for I_P^l that (except for boundary conditions and inscattering) involves only nodes upstream of P, so the solution for I_P^l can be marched from the upstream boundary to the downstream boundary of the computational domain. The price paid for the simplicity and convenience of such a scheme is loss of accuracy. For points like $u1$ in Fig. 3b that lie on an upstream plane, the bilinear interpolation for I_{u1}^l is second-order accurate with spatial grid refinement, while approximating $I_{u1^*}^l$ by $I_{u1^{**}}^l$ results in a first-order accurate estimate. Since the resulting radiant energy transfer (summed over all l) involves some first and some second-order approximations, the discretization error in the heat transfer prediction is expected to reduce with refinement of the spatial grid at a rate between first and second order.

Final Form of Governing Equation

Replacing each I_f^l values in Eq. (4) by Eq. (5), in which I_{uf}^l is found by the method just described, and where both R_f^l and $(\partial R_f^l/\partial s)_f$ are assumed known (see following section), the following equation for I_P^l results:

$$a_P^l I_P^l = a_A^l I_A^l + a_B^l I_B^l + a_C^l I_C^l + a_D^l I_D^l$$

$$+ a_E^l I_E^l + a_F^l I_F^l + a_G^l I_G^l + b_P^l \qquad (7)$$

This equation is valid for those s^l directions (shown in Fig. 3b) where the nodes included all lie upstream of P, and where all other terms have been lumped into b_P^l.

Evaluation of R_f^l and $(\partial R^l/\partial s^l)_f$

Completion of the model requires evaluation of R_f^l and its directional derivative, along s^l, for each integration point f. R_f^l values within the medium and on the boundary were simply found by interpolation and extrapolation, respectively, using values of R^l stored at nodes. The directional derivative at each f has three components, one along each coordinate direction. In the present implementation of the FVM, only the component normal to the surface was retained. This was done to simplify the algebra, and in recognition that neither the formal accuracy of the method nor its ability to capture the diffuse limit is affected. The directional derivative term was therefore estimated from the nodal point values straddling the face from a central difference approximation. The values of R_f^l and its directional derivative are therefore easily expressed in terms of nodal values like R_P^l.

To calculate the nodal values of R_P^l by Eq. (6) requires that $I_{b,P}$ and $\bar{I}_P^l$ be known. $I_{b,P}$ follows immediately from the temperature at P. To evaluate $\bar{I}_P^l$ from Eq. (2) requires accounting for inscattering from all directions s' towards s. Because ω^l is the solid angle centered on s^l, and $I(s)$ is taken as constant over ω^l and equal to I^l, so too is $\omega^{l'}$ centered on $s^{l'}$, and $I(s')$ is constant over $\omega^{l'}$ and equal to $I^{l'}$. Carrying out the 4π integration indicated in Eq. (2) to obtain $\bar{I}(s)$, then carrying out the integration of this $\bar{I}(s)$ over ω^l to obtain $\bar{I}^l$, $\bar{I}_P^l$ is given by

$$\bar{I}_P^l = \frac{1}{4\pi} \sum_{l'} I_P^{l'} \bar{\Phi}(\omega^{l'}, \omega^l) \tag{8a}$$

where the summation includes all solid angles, and where

$$\bar{\Phi}(\omega^{l'}, \omega^l) = \frac{1}{\omega^l} \int_{\omega^l} \int_{\omega^{l'}} \Phi(s', s)\, d\omega'\, d\omega \tag{8b}$$

The phase function $\Phi(s', s)$ is given by some model, so $\bar{\Phi}(\omega^{l'}, \omega^l)$ is obtained by analytical or numerical integration. For precise conservation of scattered energy, it is important that this integration be accurately performed.

Usually scattering calculations assume that the phase function depends only on the angle ψ between s' and s and not on the absolute incident (s') and scattering (s) directions. Through Eq. (8b), the present FVM easily accommodates Φ distributions that depend on absolute directions, and this permits relatively easy radiant calculations in matrices, such as insulation or foamed ceramics.

Boundary Conditions

In this analysis all boundaries are assumed diffuse-gray. For a surface at temperature T_B the boundary condition for the surface intensity, I_B, radiating into the medium, is

$$I_B = \left[(1 - \varepsilon_B) \sum_{l_{in}} Q_B^{l_{in}} + \varepsilon_B A_B \sigma T_B^4 \right] \frac{1}{\pi A_B} \tag{9}$$

The first term on the right side of Eq. (9) is the reflected component, where the summation is overall incoming radiation. The second term arises from surface emission.

Explicit Solution Procedure

The simplest solution procedure is to start with a guessed intensity field (for each location and direction), evaluate R^l, form and solve an equation such as Eq. (7) for each direction, and for each node, and use this updated intensity field as the starting point of a new iteration. This procedure converges quickly when the medium is weakly participating. Details are provided after the model is specialized to apply to axisymmetric problems.

Axisymmetric Radiation

Attention is now turned to reducing the general three-dimensional model just presented to axisymmetric problems. This is not a simple task until a mapping is understood. This section first describes the mapping, and then presents the details of how the three-dimensional model is applied.

Governing Equation

In circular cylinder coordinates (Fig. 1), the radiation intensity I depends on position $\boldsymbol{R}(r, \varphi_0, z)$ and direction $s(\theta, \phi)$. The RTE, Eq. (1) in these coordinates becomes (see Pomraning[18])

$$\left(\mu \frac{\partial}{\partial r} + \frac{\eta}{r} \frac{\partial}{\partial \varphi_0} + \xi \frac{\partial}{\partial z} - \frac{\eta}{r} \frac{\partial}{\partial \phi} \right) I(r, \varphi_0, z, \theta, \phi)$$

$$= -(K_a + \sigma_s) I(r, \varphi_0, z, \theta, \phi) + K_a I_b(r, \varphi_0, z)$$

$$+ \frac{\sigma_s}{4\pi} \int_{4\pi} I(r, \varphi_0, z, \theta', \phi') \Phi(\theta', \phi', \theta, \phi)\, d\omega' \tag{10}$$

where μ, η, and ξ are direction cosines defined as

$$\mu = \sin\theta \cos\phi, \qquad \eta = \sin\theta \sin\phi, \qquad \xi = \cos\theta \tag{11}$$

and from Fig. 1, $\phi = \varphi_r - \varphi_0$.

If axisymmetry exists, the intensity distribution becomes, by definition, invariant with φ_0 so that the RTE for the axisymmetry intensity $I(r, z, \theta, \phi)$ reduces to

$$\left(\mu \frac{\partial}{\partial r} + \xi \frac{\partial}{\partial z} - \frac{\eta}{r} \frac{\partial}{\partial \phi} \right) I(r, z, \theta, \phi) = -(K_a + \sigma_s)$$

$$\cdot I(r, z, \theta, \phi) + K_a I_b(r, z) + \sigma_s \bar{I}(r, z, \theta, \phi) \tag{12}$$

where

$$\sigma_s \bar{I}(r, z, \theta, \phi) = \frac{\sigma_s}{4\pi} \int_{4\pi} I(r, z, \theta', \phi') \Phi(\theta, \phi, \theta', \phi')\, d\omega' \tag{13}$$

Mapping for Solution of Axisymmetric Problems

Axisymmetric radiant heat transfer occurs when the intensity is independent of φ_0, and is therefore completely specified by r, z, θ, and ϕ, as just discussed. The intensities shown in Fig. 4a all have the same values of r, z, and θ. The angle $\Delta\varphi_0$ between all numbered points is $\pi/4$. The points 1, 2, 3, . . . are located at $\varphi_0 = 7\pi/8, 5\pi/8, 3\pi/8, \ldots$ respectively, and the angle φ_r is zero for each intensity. The angles $\phi = \varphi_r - \varphi_0$ for the intensities $I_1^1, I_2^1, I_3^1, \ldots$ are therefore, $-7\pi/8$, $-5\pi/8$, $-3\pi/8$ . . . .

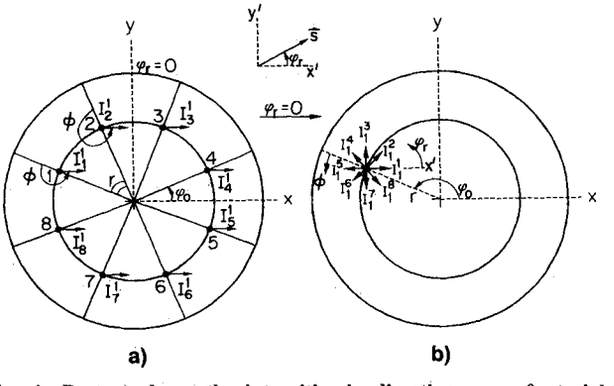

Fig. 4 Part a) shows the intensities in direction $\varphi_r = 0$ at eight locations equidistant from the axis of the cylinder. The angular distribution of the intensity field at location one appears in b).

In Fig. 4b the intensities all have the same values of r, z, and θ as in Fig. 4a, but are now all located at $\varphi_0 = 7\pi/8$, with $\varphi_r = 0, \pi/4, \pi/2, \ldots$ for the intensities $I_1^1, I_1^2, I_1^3, \ldots$. The $\phi = \varphi_r - \varphi_0$ angles are therefore $-7\pi/8, -5\pi/8, -3\pi/8, \ldots$, respectively. It follows that the values of r, z, θ, and ϕ are the same for I_j^1 in Fig. 4a and I_1^j in Fig. 4b, $j = 1, 2, 3, \ldots 8$, and (since r, z, θ, and ϕ completely specify the intensity when axisymmetry prevails) therefore, $I_j^1 = I_1^j$. A simple mapping therefore exists between the intensities in Figs. 4a and 4b; in calculating intensities it will often be easier to compute the intensities depicted in Fig. 4a.

For the integral equations for the intensities in Figs. 4a and 4b to be exactly the same, the $\Delta\varphi_0$ spacing between nodes in Fig. 4a should be uniform and equal to the $\Delta\varphi_r$ spacing between the intensity directions in Fig. 4b, and the discrete solid angle ω^l used when the FVM is applied to Fig. 4a should extend from $-\Delta\varphi_r/2$ to $+\Delta\varphi_r/2$ (see Fig. 2c). Carlson and Lathrop[19] introduced an artifice into their discrete ordinates method in order to avoid difficulties (lack of conservation and unphysical directional coupling) that arose from the third term on the left side of Eq. (12); when the FVM is applied to obtain the intensities in Fig. 4a, these problems are totally avoided.

It will be immediately recognized that the mapping just presented can be used for any number of intensity components. Furthermore the intensity distribution will usually be symmetric as well [in Fig. 4a $I(r, \varphi_0, z, \theta, \varphi_r = 0) = I(r, -\varphi_0, z, \theta, \varphi_r = 0)$] so that only the intensities for $y \geq 0$ need be calculated.

Solution Procedure

To solve an axisymmetric radiation problem in the cylinder in Fig. 2, the last section showed that it is sufficient to solve for the intensity component $I(r, \varphi_0, z, \theta, \varphi_r = 0)$. The spatial control volume P is bounded by r_{P+}, r_{P-}, $\varphi_{0,P+}$, $\varphi_{0,P-}$, z_{P+}, z_{P-}. The discrete solid angle covers the range shown in Fig. 2c (θ^{l-} to θ^{l+} and $-\Delta\varphi_r/2$ to $+\Delta\varphi_r/2$, where $\Delta\varphi_r = \Delta\varphi_0 = \varphi_{0,P+} - \varphi_{0,P-}$). Following the discretization procedure outlined earlier, an algebraic equation is written for the intensity in each direction l at each node. Each nodal intensity depends only on upstream nodal intensities.

For $\theta < \pi/2$ the solution is marched from the outer wall to the center of segment 1 in Fig. 2a for each z level beginning at the bottom and ending at the top (maximum z). The boundary condition along the symmetry surface ($y = 0$ in Fig. 2a) is $Q^l = 0$, because the computed intensities transport no heat across this surface. The solution in the adjacent segment is likewise found, and the process is repeated for all segments in the quadrant I [$(\pi/2) \leq \varphi_0 \leq \pi$]. The solution in quadrant II is similar except the sweep is from the center towards the outer wall in order to keep the marching direction the same as s^l. When all nodal values have been updated, a new solution for intensity has been created for one angle θ^l. The process is repeated for each θ^l, being careful to reverse the sweep direction in the z direction for $\theta > \pi/2$.

The nodal intensities just obtained constitute the desired solution if the enclosure walls are black, the medium temperature is known, and there is no scattering. Otherwise these intensities are used to update the radiant flux leaving the wall, the medium temperature, and the scattering. The solution for updated intensities is embedded in an outer iteration loop that is repeated until the solution converges.

Methods of updating these variables are described by Raithby and Chui.[13] In the present study the medium temperature is assumed known. The gray-wall boundary conditions and the intensities used in the inscattering calculation were updated at the end of each outer loop.

Results

To evaluate the performance of the FVM it is desirable to compare its predictions to exact results and the predictions of earlier models. Most of the results presented here are therefore for "clean," benchmark-type, problems.

Comparisons with Exact Solutions

Enclosure with an Absorbing-Emitting Medium

The first test case involves a cylindrical enclosure (see Fig. 5) containing an absorbing-emitting but nonscattering medium at constant temperature ($T_M = 100$ K). It has a height of $z_c = 2$ m and radius $r_c = 1$ m. The walls are assumed cold ($T_w = 0$) and black ($\varepsilon_w = 1$). The objective is to compare the FVM prediction of the total radiant heat transfer on the radial wall q_r with an exact solution obtained as follows.

In the absence of scattering the intensity at any location within the cylinder is, from the following solution to Eq. (1)

$$I(r, z, \theta, \phi) = I_b(1 - e^{-K_a S}) \tag{14}$$

where S is the distance upstream to the vessel wall along the ray defined by (θ, ϕ), and $I_b = (\sigma T_M^4)/\pi$ is the black body intensity of the homogeneous medium. To obtain the "exact" radiant flux q_r, emitted from the gas and falling on the radial wall, the heat flux at each point on the wall was obtained by numerically integrating $I(s \cdot n)$ over all incident solid angles. The dimensionless radiant flux $q_r^* = q_r/\sigma T_M^4$, from the middle of the cylinder side to the end, is shown in Fig. 5 as solid lines for three optical thicknesses ($\kappa^* = K_a r_c = 0.1, 1.0, 5.0$).

The finite volume solution to this problem at discrete locations along the cylinder side is also plotted in Fig. 5. The prediction was based on a moderately fine grid: 16 control volumes in the r direction ($N_r = 16$), 30 in the z direction ($N_z = 30$), 12 polar angles ($N_\theta = 12$), and 16 azimuthal angles ($N_\phi = 16$); an error of less than 0.2% was obtained for all three optical thicknesses. This accuracy of the FVM is somewhat better than that of the spherical harmonic (P_3) method by Mengüç and Viskanta,[6] also shown in Fig. 5 (as dashed lines); their prediction is based on a grid $N_r \times N_z = 21 \times 41$.

The same test problem was used to study the reduction in the discretization error with grid refinement for the present method. Figure 6 displays the error curves for the prediction of the dimensionless total radiant flux $Q_r^* = (\int_{z=0}^{2} q_r^* \, dz)$ for $\kappa^* = 5$. These curves are generated by varying the components of the spatial and angular grids (i.e., N_r, N_z, N_θ, N_ϕ) one at a time from the mesh $N_r = 16$, $N_z = 30$, $N_\theta = 12$, $N_\phi = 16$ that gives the almost exact total flux (error ~ 0.003%). The discretization error is seen to decrease quadratically with

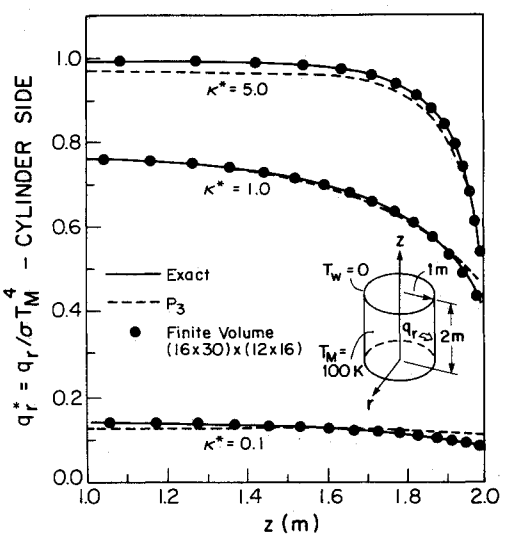

Fig. 5 Nondimensional radiant heat transfer on the side wall of a cylindrical enclosure containing an absorbing emitting, but nonscattering, gas at uniform temperature T_M with zero wall temperature for three optical thicknesses $\kappa^* = K_a r_c = 0.1, 1.0, 5.0$.

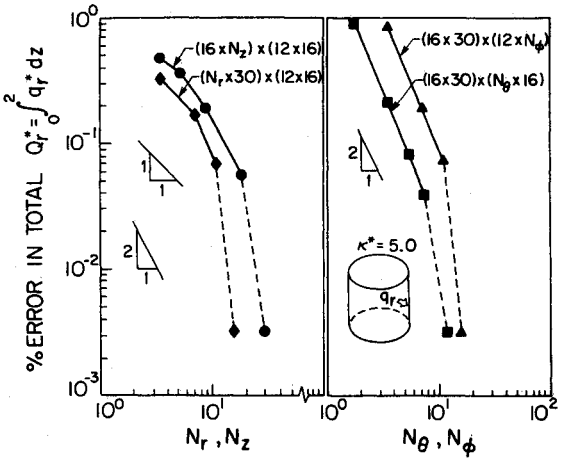

Fig. 6 Reduction in the error of total radiant heat transfer to the side of the cylindrical enclosure with spatial refinement (left side) and angle refinement (right side).

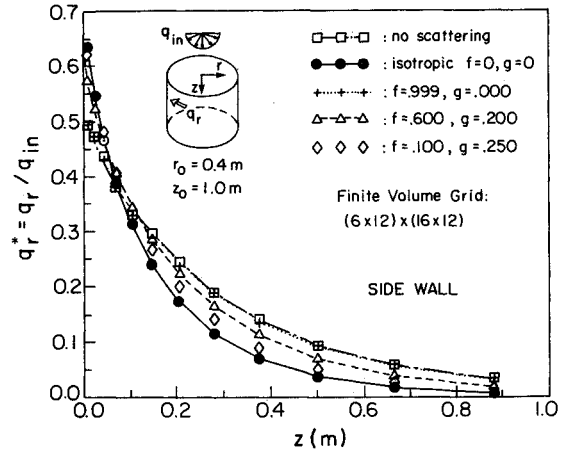

Fig. 7 Nondimensional radiant heat transfer on the radial wall of a cylindrical enclosure with a diffuse radiant flux q_{in} on the top wall for a scattering medium. The base case 1 has no scattering $\sigma_s = 0$, $K_a = 0.5\ m^{-1}$. Cases 2–5 incorporate four different scattering phase functions, all with $\sigma_s = 5\ m^{-1}$ and $K_a = 0.5\ m^{-1}$.

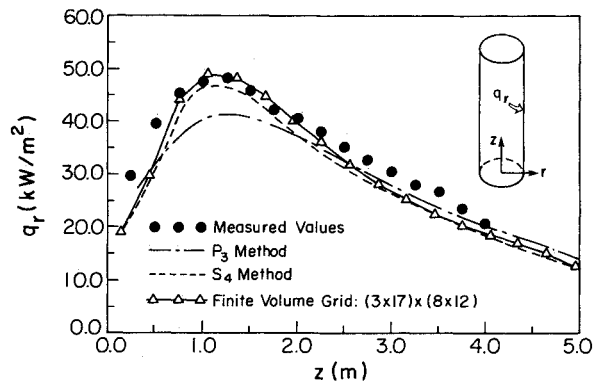

Fig. 8 Comparison of local radiant fluxes at the side wall of a cylindrical furnace obtained from the finite volume method, P_3 approximation (Mengüç et al.[6]), and S_4 method (Fiveland[4]) with experimental data (Wu et al.[25]).

the angular refinement (i.e., increased N_θ and N_ϕ). The error reduction with the refinement of the spatial grid is somewhere between linear and quadratic, as previously anticipated. Typically the fine grid solutions (error < 0.01%) required a CPU time of 450 s on a VAX 11-785 machine, while coarser grid solutions (error ~ 1%), required about 80 s.

Enclosures with Absorbing-Isotropically Scattering Media

The second benchmark case involves a finite cylindrical enclosure with cold black walls subject to a diffuse radiant emission in from the top circular wall. The enclosed medium is assumed to be homogeneous, absorbing, isotropically scattering, but nonemitting. The analytical formulation for this problem, was presented by Crosbie and Farrell,[20] and exact solutions at six specific test conditions have been made available by Crosbie.[21] The six test conditions included enclosures of three different sizes with various magnitudes of scattering and absorption coefficients. The accuracy of the FVM has been checked by making comparisons to these solutions for the case $\sigma_s = K_a$ and with $(\sigma_s + K_a)r_c = 1$ and 5.

Space limitations do not permit a graphical presentation of comparisons (see Chui[22]). For a cavity radius to height ratio of 5, the heat fluxes on all surfaces were predicted to within 5% for a coarse mesh ($N_r = 6$, $N_z = 4$, $N_\theta = 8$, $N_\phi = 4$); the CPU time was about 10 s on a VAX 11-785. Doubling the grid size sharply reduced the error and increased CPU time by a factor of 15.

Similar results were found for other cavity aspect ratios. For a tall thin cylinder (radius to height of 0.1) the finite volume results on a coarse mesh ($N_r = 4$, $n_z = 12$, $N_\theta = 6$, $N_\phi = 4$) were distinctly better than for the P_3 method.[6]

Anisotropic Scattering

The FVM was again applied to a cylindrical geometry (see Fig. 7), but anisotropic scattering was included. The cylinder has height $z_0 = 1$ m, radius $r_0 = 0.4$ m, and emits diffuse radiation from the top surface at a uniform rate q_{in}. The walls are cold and black, the medium is cold (nonemitting), and (in all but the baseline case) absorbs $K_a = 0.5\ m^{-1}$ and scatters $\sigma_s = 5\ m^{-1}$ anisotropically in accordance with the delta-Eddington phase function (Joseph and Wiscombe[23]; Crosbie and Davidson[24])

$$\Phi(\psi) = 2f\delta(1 - \cos\psi) + (1 - f)(1 + 3g\cos\psi) \quad (15)$$

where ψ is the angle between the incident and scattered directions. The first term on the right side contains the delta function; f governs the amount of forward scattering, g governs the degree of asymmetry about $\psi = \pm\pi/2$, and there is symmetry about $\psi = 0$. The computational grid used was ($N_r \times N_z$) = (6 × 12) and ($N_\phi \times N_\theta$) = (16 × 12). Predictions of the nondimensional heat flux distribution on the side wall (Fig. 7) are shown for five different scattering conditions. The baseline case of no scattering (square symbols), $\sigma_s = 0$, $K_a = 0.5\ m^{-1}$ results in a high heat load, for $z \geq 0.1$ m, on the radial surface. The other limiting case is isotropic scattering, $\sigma_s = 5\ m^{-1}$, $K_a = 0.5\ m^{-1}$ which results in minimum net heat transfer on the radial surface for $z \geq 0.1$ m. As f is increased from 0.1 to 0.999, the amount of forward scattering increases, increasing the amount of radiation that reaches the lower regions of the cavity. For $f = 0.999$, $g = 0.0$, nearly all scattering is forward so the nonscattering baseline case should be recovered; the FVM captures the expected behavior extremely closely to the side wall (Fig. 7) and top and bottom walls (not shown). For $f = 0.1$ and low asymmetry ($g = 0.25$) the predictions lie, as they should, close to the isotropic limit.

It can be concluded that the model predictions in this test follow correct trends.

Comparison with Measured Furnace Data

The last test involves the application of the method to predict the radiative heat transfer in an International Flame Research Foundation test furnace (see Fig. 8). Experimental radiant flux data along the lateral side of the cylindrical furnace and the temperature of the medium have been obtained by Wu and Fricker.[25] The objective is to predict the net radiant heat transfer in the radial direction q_r on the furnace side wall, given the measured temperature data.

The spherical harmonic (P_3) method has been applied to this problem by Mengüç and Viskanta[6] and the discrete or-

dinate method by Fiveland,[4] both using $K_a = 0.3\ m^{-1}$ and $\sigma_s = 0$, and their results are also shown in Fig. 8. Using the same temperature data, similar grid $(N_r \times N_z) \times (N_\theta \times N_\phi) = (3 \times 17) \times (8 \times 12)$, and identical K_a and σ_s, the FVM yielded the results shown for comparison on this figure. It is tempting to claim that the present results are slightly better than those from the other models, but the accuracy of the prediction depends on the values of K_a and σ_s used, and their correct values are not known (nor are they constant). Suffice it to claim that the FVM is able to reproduce a physically reasonable radiant flux distribution that follows the trend of the measured data, peaking between $z = 1$ to 1.5 m.

Summary

Application of the finite volume method has been described for problems in which radiant intensity varies over three space dimensions and two angles. In this application consideration has been restricted to cases with circular-cylinder computational meshes. A special discretization was used that slightly sacrificed accuracy to gain simplicity and economy in solving the radiation transfer equation. The proposed formulation can potentially incorporate any scattering phase function.

It has also been shown that, when the radiation problem is axisymmetric, a special mapping can be used to transform the dependence of intensity on two space coordinates and two angles, to three space coordinates and one angle. In this analysis the general finite volume method has been specialized to apply to such problems.

Predictions for several axisymmetric benchmark problems and one furnace problem show that the present method is quite accurate for coarse grids, that the error decreases rapidly as the grid is refined, and that the solutions are inexpensively obtained.

Acknowledgments

This work was supported by a contract from the Combustion and Carbonization Research Laboratory, CANMET, of the Energy Mines and Resources Department of the Canadian Federal Government. Special thanks are extended to K. G. T. Hollands of the Mechanical Engineering Department at the University of Waterloo for his instructive comments and useful suggestions. We also wish to acknowledge the assistance of Professor Crosbie, who supplied publications as well as unpublished results.

References

[1]Perlmutter, M., and Howell, J. R., "Radiant Transfer Through a Grey Gas Between Concentric Cylinders Using Monte Carlo," *Journal of Heat Transfer,* Vol. 86, 1964, pp. 165–179.

[2]Lowes, T. M., Bartelds, H., and Heamp, M. P., Michelfelder, S., and Pai, B. E., "Prediction of Radiant Heat Flux Distribution," *Heat Transfer in Flames,* edited by N. H. Afgan and J. M. Beer, Scripta, Washington, DC, 1974, pp. 179–190.

[3]Steward, F. R., and Tennankore, K. N., "Towards a Finite Difference Solution Coupled with the Zone Method for Radiative Transfer for a Cylindrical Combustion Chamber," *Journal of the Institute of Energy,* Sept. 1979, pp. 107–114.

[4]Fiveland, W. A., "A Discrete Ordinates Method for Predicting Radiative Heat Transfer in Axisymmetric Enclosure," American Society of Mechanical Engineers Paper 82-HT-20, 1982.

[5]Fernandes, R., and Francis, J., "Combined Conductive and Radiative Heat Transfer in an Absorbing, Emitting, and Scattering Cylindrical Medium," *Journal of Heat Transfer,* Vol. 104, 1982, pp. 594–601.

[6]Mengüç, M. P., and Viskanta, R., "Radiative Transfer in Axisymmetric, Finite Cylindrical Enclosures," *Journal of Heat Transfer,* Vol. 108, 1986, pp. 271–276.

[7]Jamaluddin, A. S., and Smith, P. J., "Predicting Radiative Transfer in Axisymmetric Cylindrical Enclosures Using the Discrete Ordinates Method," *Combustion Science and Technology,* Vol. 62, 1988, pp. 173–186.

[8]Yucel, A., and Williams, M. L., "Interaction of Conduction and Radiation in Cylindrical Geometry with Azimuthal Symmetry," *Proceedings of the 1988 National Heat Transfer Conference,* American Society of Mechanical Engineers, HTD-Vol. 96, Houston, TX, pp. 281–289.

[9]Carvalho, M. G., Farias, T., and Francis, P. "Predicting Radiative Heat Transfer in Absorbing, Emitting, and Scattering Media Using the Discrete Transfer Method," *Proceedings of the 1991 National Heat Transfer Conference,* American Society of Mechanical Engineers, HTD-Vol. 160, Minneapolis, MN, pp. 17–26.

[10]Howell, J. R., "Thermal Radiation in Participating Media: The Past, the Present, and Some Possible Futures," *Journal of Heat Transfer,* Vol. 110, 1988, pp. 1220–1226.

[11]Viskanta, R., and Mengüç, M. P., "Radiative Heat Transfer in Combustion Systems," *Progress in Energy and Combustion Science,* Vol. 13, No. 2, 1987, pp. 97–160.

[12]Carlson, B. G., and Lathrop, K. D., "Transport Theory—the Method of Discrete Ordinates," *Computing Methods in Reactor Physics,* edited by H. Greenspan, C. N. Kelber, and D. Okrent, Gordon and Breach, New York, 1968, p. 171.

[13]Raithby, G. D., and Chui, E. H., "A Finite-Volume Method for Predicting Radiant Heat Transfer in Enclosures with Participating Media," *Journal of Heat Transfer,* Vol. 112, 1990, pp. 415–423.

[14]Fiveland, W., "Three-Dimensional Radiative Heat Transfer Solutions by the Discrete-Ordinate Method," *Journal of Thermophysics and Heat Transfer,* Vol. 2, No. 4, 1988, pp. 309–316.

[15]Lathrop, K. D., "Remedies for Ray Effects," *Nuclear Science and Engineering,* Vol. 45, 1971, pp. 255–268.

[16]Siegel, R., and Howell, J. R., "Thermal Radiation Heat Transfer," 2nd ed., McGraw-Hill, New York, 1981, pp. 437–438.

[17]Heubner, K. H., "The Finite Element Method for Engineers," Wiley, New York, 1975.

[18]Pomraning, G. C., "The Equations of Radiation Hydrodynamics," Pergamon, Oxford, England, UK, 1973, p. 84.

[19]Carlson, B. G., and Lathrop, K. D., "Transport Theory—The Method of Discrete Ordinates," *Computing Methods in Reactor Physics,* edited by H. Greenspan, C. N. Kelber, and D. Okrent, Gordon and Breach, New York, 1968, pp. 183–184.

[20]Crosbie, A. L., and Farrell, J. B., "Exact Formulation of Multiple Scattering in a Three-Dimensional Cylindrical Geometry," *Journal of Quantitative Spectroscopy and Radiative Transfer,* Vol. 31, No. 5, 1984, pp. 397–416.

[21]Crosbie, A. L., private communication, Dept. of Mechanical and Aerospace Engineering, Univ. of Missouri, Rolla, MO, 1989.

[22]Chui, E. H., "Modelling of Radiative Heat Transfer in Participating Media by the Finite Volume Method," Ph.D. Thesis, Dept. of Mechanical Engineering, Univ. of Waterloo, Waterloo, Ontario, Canada, 1990.

[23]Joseph, J. H., and Wiscombe, W. J., "The Delta-Eddington Approximation for Radiative Heat Transfer," *Journal of Atmospheric Sciences,* Vol. 33, 1976, pp. 2452–2459.

[24]Crosbie, A. L., and Davidson, G. W., "Dirac-Delta Function Approximations to the Scattering Phase Function," *Journal of Quantitative Spectroscopy & Radiative Transfer,* Vol. 33, No. 4, 1985, pp. 391–409.

[25]Wu, H. L., and Fricker, N., "The Characteristics of Swirl-Stabilized Natural Gas Flames. Part 2: The Behaviour of Swirling Jet Flames in a Narrow Cylindrical Furnace," *Journal of the Institute of Fuel,* Vol. 49, 1976, pp. 144–151.